PAPER

Nonlinear features of guided wave scattering from rivet hole nucleated fatigue cracks considering the rough contact surface condition

Nonlinear features of guided wave scattering from rivet hole nucleated fatigue cracks considering the rough contact surface condition

Yanfeng Shen[1] , Junzhen Wang[1] and Wu Xu[2]

[1] University of Michigan-Shanghai Jiao Tong University Joint Institute, Shanghai Jiao Tong University, Shanghai, 200240, People's Republic of China
[2] School of Aeronautics and Astronautics, Shanghai Jiao Tong University, Shanghai, 200240, People's Republic of China

E-mail: yanfeng.shen@sjtu.edu.cn

Abstract

This article presents the investigation of nonlinear scattering features of guided waves from rivet hole nucleated fatigue cracks considering the rough contact surface condition. A small-size numerical model based on the local interaction simulation approach is developed, enabling the efficient analysis of the contact acoustic nonlinearity during the wave crack interactions. The study starts with an idealized breathing crack model possessing smooth, perfectly kissing contact surfaces. Then, the nature of rough crack surfaces is considered with randomly distributed initial openings and closures. Several distinctive aspects of the nonlinear scattering phenomenon are discussed: (1) the amplitude effect, which renders significantly different nonlinear response under various levels of excitation wave amplitudes; (2) the directivity and mode conversion features, which addresses the scattering direction dependence of the fundamental and superharmonic wave mode components; (3) the nonlinear resonance phenomenon, which maximizes the nonlinear response during the wave crack interactions at certain excitation frequency ranges. This study demonstrates that these nonlinear features are substantially influenced by the crack surface condition and differ much between an idealized breathing crack and a rough crack in most practical cases. Fatigue tests on a thin aluminum plate with a rivet hole is conducted to induce cracks in the specimen. An active sensor array surrounding the crack zone is implemented to generate and receive ultrasonic guided waves in various directions. Current work emphasizes on using a highly efficient numerical model to explain the nonlinear features of scattered waves from fatigue cracks considering the rough crack surface condition. These special features may provide insights and guidelines for nonlinear guided wave based nondestructive evaluation and structural health monitoring system design. The paper finishes with discussion, concluding remarks, and suggestions for future work.

Keywords: structural health monitoring, nondestructive evaluation, nonlinear ultrasonics, local interaction simulation approach, scattering, breathing crack, fatigue crack

(Some figures may appear in colour only in the online journal)

1. Introduction

Fatigue cracks exist as great menace to engineering structures, because they are barely visible and hard to detect. Thus, the development of effective fatigue crack detection methodologies is of critical importance. Among current solutions, ultrasonic inspection technology has been found to be promising. Compared with linear ultrasonic techniques which are sensitive to gross defects, the nonlinear counterpart, on the other hand, proves to be more sensitive to incipient changes such as fatigue cracks. When guided waves interact with fatigue cracks, contact acoustic nonlinearity (CAN) would arise, which may introduce distinctive signal features, such as sub/super harmonic generation, DC response, mixed frequency modulation response (sideband effects), and various frequency/amplitude dependent threshold behaviors [1]. As a consequence, nonlinear guided wave based inspection techniques are drawing increasing attention among the structural health monitoring (SHM) and nondestructive evaluation (NDE) communities, because it inherits both the sensitivity from nonlinear ultrasonics and the large-area inspection capability of guided waves [2].

Many researchers have explored using guided waves for crack detection. Some of them focused on the linear scattering features. Alleyne and Cawley studied the interaction of Lamb waves with notch-like defects using the finite element method (FEM) and experiments [3]. Rose *et al* explored the guided wave inspection techniques for nuclear steam generator tubing [4]. Kundu *et al* conducted a series of original research on using guided waves for damage detection in plates and laminated composites [5–8]. The guided wave scattering analysis also enabled the identification of discontinuity in concrete [9]. Damage detection methodologies using guided waves were also studied for underwater or buried pipes [10–12]. Fromme investigated ultrasonic guided wave scattering for fatigue crack characterization using non-contact measurements [13]. Chan *et al* continued this high frequency guided wave laser testing approach to monitor the fatigued crack growth in multi-layer model aerospace structures [14]. Chen *et al* utilized a sparse sensor array to estimate the scattering pattern of guided waves from fatigue cracks [15]. To further analyze the scattering of Lamb waves from a fastener hole with a fatigue crack, Masserey and Fromme conducted both finite difference modeling and experiments with laser interferometer [16]. Quaegebeur *et al* proposed an experimental technique to measure the scattering pattern from geometric discontinuities, where they found the scattering pattern from a fatigue crack differed much from that of a machined notch [17]. This indicates that the closed rough fatigue crack surface will impose significant influence on the scattered wave field. In addition to the investigations on the linear scattering features at fatigue cracks, the nonlinear counterpart has also drawn considerable attention. Klepka *et al* adopted the nonlinear acoustics and wave modulation technique to identify fatigue cracks [18]. Utilizing the load-differential effect, Chen *et al* took advantage of the crack close status under varying loading conditions to image the fatigue crack [19]. Hong *et al* achieved accurate localization of a fatigue crack by the temporal nonlinear signal features [20]. Wu *et al* explored using the nonlinear amplitude effect to construct instantaneous baseline for fatigue crack detection with the tomography imaging algorithm [21]. Liu *et al* extracted the fatigue crack information using the non-contact measurements and nonlinear modulation method, which allowed the visualization of fatigue cracks using the scanning laser vibrometry [22, 23]. Lim *et al* further conducted the study to develop the field application of the baseline free nonlinear ultrasonic modulation approach and successfully detected the fatigue crack [24]. Cheng *et al* quantified the fatigue crack using a nonlinear ultrasonic phased array imaging technique and found the nonlinearity of the sensing signals increases with the fatigue crack length [25].

Many modeling methodologies have been developed to investigate the nonlinear wave crack interactions [26]. Analytical models are computationally efficient and allow fast parametric studies, but they are confined by the complexity of structures and damage types [27]. To fully capture the 3D nonlinear dynamics, FEM for contact-impact problems has been widely investigated, maturing over the years [28]. The nonlinear scattering of bulk waves from closed cracks has been investigated, such as the time domain boundary integral equation given by Hirose and the nonlinear spring analytical model given by Poznic and Pecorari [29, 30]. A recent contribution is from Blanloeuil *et al* using FEM and extended analytical approach [31, 32]. On-going research by Wang and Su is being conducted as an effort to model CAN during the nonlinear interactions between guided waves and a breathing crack [33, 34]. Hafezi and Kundu recently contributed the peri-ultrasonic modeling technique to solve the linear and nonlinear wave scattering problems [35, 36]. He and Ng used a time-domain spectral FEM for the modeling and analysis of nonlinear guided wave interaction with a breathing crack [37]. The development of local interaction simulation approach (LISA) into the nonlinear region makes it possible to analyze nonlinear interactions between guided waves and fatigue cracks in a highly efficient manner [38–40]. Most of the state-of-the art simulation efforts adopted the idealized breathing crack model, where the crack surfaces are smooth kissing interfaces. Nevertheless, such an assumption deviates from the practical crack features and may result in much difference in the predictive results. It should be noted that pioneer modeling investigations on the linear scattering of longitudinal wave from rough crack-like defects have been conducted [41]. However, this research effort differs from the previous investigations by marching into the nonlinear region of the scattering phenomena of multimodal Lamb waves considering the rough contact interfaces of the fatigue cracks.

In this study, a small-size LISA model is tailored for the analysis of nonlinear scattering of guided waves from fatigue cracks. First, the directivity and mode conversion features are discussed for an idealized breathing crack model. Then, the rough crack surface with initial openings and closures is considered. The mechanism of amplitude effect of the nonlinear scattering is analyzed by comparing the breathing crack and rough crack ultrasonic responses. Subsequently, the random directivity and mode conversion features are noticed,
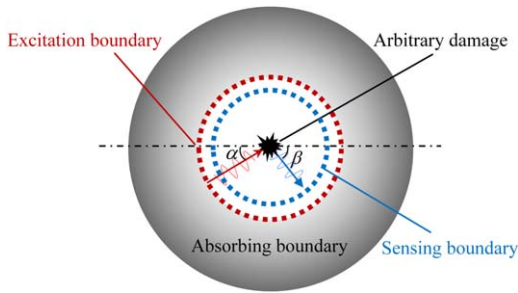
Figure 1. Small-size LISA model for guided wave scattering analysis.

which differ much from the breathing crack case. Finally, the nonlinear resonance phenomenon will be explored using a chirp excitation. Distinctive subharmonic and superharmonic components are observed at the resonant frequencies. The rough surface condition imposes considerable influence on the nonlinear resonance phenomena. Experiments on an aluminum plate with a rivet hole nucleated fatigue crack are conducted and the major trends for the above three aspects of nonlinear wave crack interactions are compared with the numerical analysis.

2. Small-size LISA model for guided wave scattering analysis

LISA is a finite-difference based numerical simulation method. It approximates the partial differential elastodynamic equations with finite difference quotients in the discretized temporal and spatial domains. The final iterative equations (IEs) determine the displacements of a certain node at current time step based on the displacements of its eighteen neighboring nodes at previous two/three time steps, depending on whether material damping is considered. For details of the derivation for the LISA IEs, the readers are referred to [42]. A penalty method was deployed to introduce contact dynamics into LISA. When the crack surfaces come into contact, contact forces are applied on the contact nodes to constrain the in-contact motion. Thus, the modeling of the alternating boundary (crack open and close) condition can be achieved. A Coulomb friction model was integrated to capture the stick-slip contact motion. The details of the contact LISA formulation and the guidelines for the proper choice of computational parameters for an accurate and converged solution are given in [38].

Figure 1 presents the small-size LISA model tailored for guided wave scattering analysis. The model is comprised of an interior region with the damage at the center and an exterior region extended with absorbing layers. Since LISA belongs to the family of numerical methods with spatial and temporal discretization, such model is capable of describing arbitrary damage profiles. The red circle represents the excitation points where guided waves can be generated from an arbitrary incident angle. The blue circle layouts the sensing points picking up the scattered waves in each direction. The absorbing boundary is implemented using the absorbing

layers with increasing damping (ALID) method [43]. It allows the simulation of wave propagation in an infinite domain with a finite dimensional model. The guided waves directly generated by the excitation points and those scattered by the damage are absorbed by the silent boundary setup.

Single mode guided waves are generated at the excitation points by exerting in-phase or out-of-phase out-of-plane traction forces at the top and bottom surfaces of the plate. The contact problem is solved using the transient dynamic analysis. A continuous harmonic excitation is gradually introduced into the model to generate guided waves at the frequency of interest. Guided waves will impinge on the damage and nonlinear interactions may take place. Scattering and mode conversion will happen as well. The scattered waves will radiate outward and be picked up by the sensing points and are finally absorbed by the ALID boundary. In order to perform the quantitative analysis of the nonlinear scattering features, the sensing points across the plate thickness are all employed. The motion of the points across the thickness allows the decomposition of the guided waves modes using the wave mode shapes. In this way, the model allows the evaluation of the scattered wave modes in a quantitative manner.

There are two aspects that make this model computationally efficient: (1) the size of the model is minimized by employing the absorbing boundary, which considerably alleviates the computational burden; (2) the LISA model is implemented using the compute unified device architecture (CUDA) technology and executed massively in parallel on powerful graphics cards, which facilitates the high performance in computing.

In order to evaluate the nonlinear scattering phenomenon, the scattering coefficients can be extracted using modal expansion technique based on guided wave mode shapes calculated from the semi-analytical finite element method. The wave damage interaction coefficients (WDICs) were adopted to quantify the participation of each guided wave mode during the scattering procedure. A typical WDIC can be expressed as $C_{IN-N}(\alpha, \beta, f_n)$. The two sub-indices are used to designate the incident wave mode (IN) and the scattered wave mode (N), respectively. α and β are the incident angle and scattered direction as given in figure 1. f_n represents the harmonic frequency component, i.e., f_1 represents fundamental excitation frequency, while f_2 and f_3 represents second and third higher harmonic frequencies, respectively. For instance, if the incident wave frequency is at 100 kHz, then $C_{S0-A0}(30, 150, 200)$ represents the second harmonic frequency (200 kHz) scattering coefficient of mode converted A0 waves in 150° direction resulted from an oblique 30° S0 incident wave; $C_{A0-SHS0}(0, 180, 300)$ designates the scattering coefficient of mode converted fundamental symmetric shear horizontal mode (SHS0) at the third harmonic in 180° direction due to the 0° incident A0 mode incidence at the damage. Details about the definition and derivation of WDICs can be found in [44, 45].
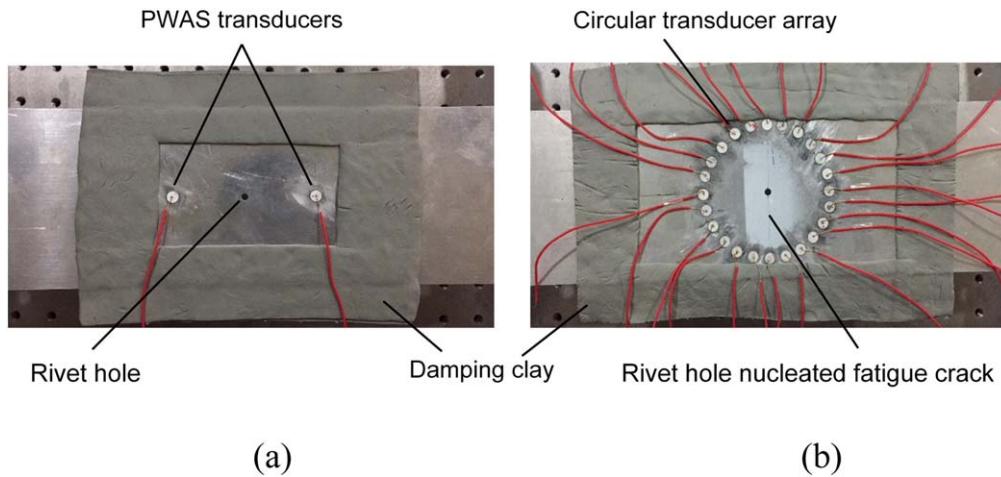
Figure 2. Specimens for the ultrasonic active sensing tests: (a) aluminum plate with a pristine rivet hole; (b) aluminum plate with rivet hole nucleated fatigue cracks.

3. Experimental setup on wave crack nonlinear interactions

In addition to the modeling efforts, guided wave active sensing experiments on a fatigue specimen were also carried out. Figure 2 shows the specimens used for the investigation. In order to demonstrate the nonlinear effects caused by the interactions between guided waves and the fatigue crack, an aluminum plate with a pristine rivet hole was also prepared as the comparative case. Both specimens were machined from a 1 mm thick 2024 aluminum plate. A 4 mm diameter rivet hole was machined on both plates. One of the plates was loaded using the fatigue test facility. The fatigue specimen was subjected to a total number of 350 000 cycles with load control. The fatigue cracks were nucleated on both sides of the rivet hole and grow outwards. A 30 mm long fatigue crack was finally obtained on each side of the hole. On the pristine plate, a pair of piezoelectric wafer active sensors (PWAS) were bonded, forming a pitch-catch active sensing configuration. On the fatigued plate, a circle of 24 PWAS transducers were mounted as a sensor array to generate and receive guided waves at every 15° angle. Damping clay was implemented surrounding the active sensing area to absorb boundary reflections.

Figure 3 presents the experimental setup for the nonlinear ultrasonic tests. A Keysight 33500B arbitrary function generator was used to generate excitation waveforms. The excitation signal was further amplified by a Krohn-hite 7602M wideband power amplifier and was applied on the transmitter PWAS. Guided waves were generated, propagated along the plate, interacted with the crack, and were finally picked up by the receiver PWAS. The sensing waveforms were collected by the Keysight DSO-X 3014T digital storage oscilloscope. When one PWAS was used as the transmitter, all the other transducers performed as sensors, recording the structural response. Thus, the scattered information can be obtained in every 15° direction. Since the frequency domain information is of particular interest for the nonlinear ultrasonic study, excitations with a large number of counts are desired to obtain
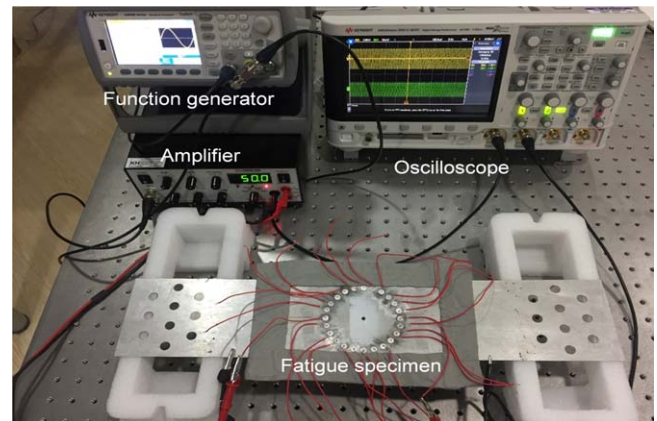

Figure 3. Experimental setup for the nonlinear ultrasonic tests.

high resolution frequency domain details. In the experiments, continuous harmonic excitations were used. Comparative study between the pristine rivet hole and the fatigued rivet hole with cracks were first conducted. The amplitude effect in the nonlinear ultrasonic inspections were investigated by applying various levels of excitations. Then, the scattering patterns for the superharmonic components were obtained to study the scattering directivity. Finally, to investigate the nonlinear resonance effect, frequency sweeping experiments were carried out. The numerical modeling analysis and experimental evaluation results will be shown in the following section.

4. Conventional idealized breathing crack model results

Our analysis starts with the idealized breathing crack model, the prevailing practice to study the nonlinear wave crack interactions, where the crack surfaces are considered to be smooth in perfectly kissing contact condition without initial gap nor pre-stresses. Figure 4 presents the numerical simulation results of nonlinear interactions between the
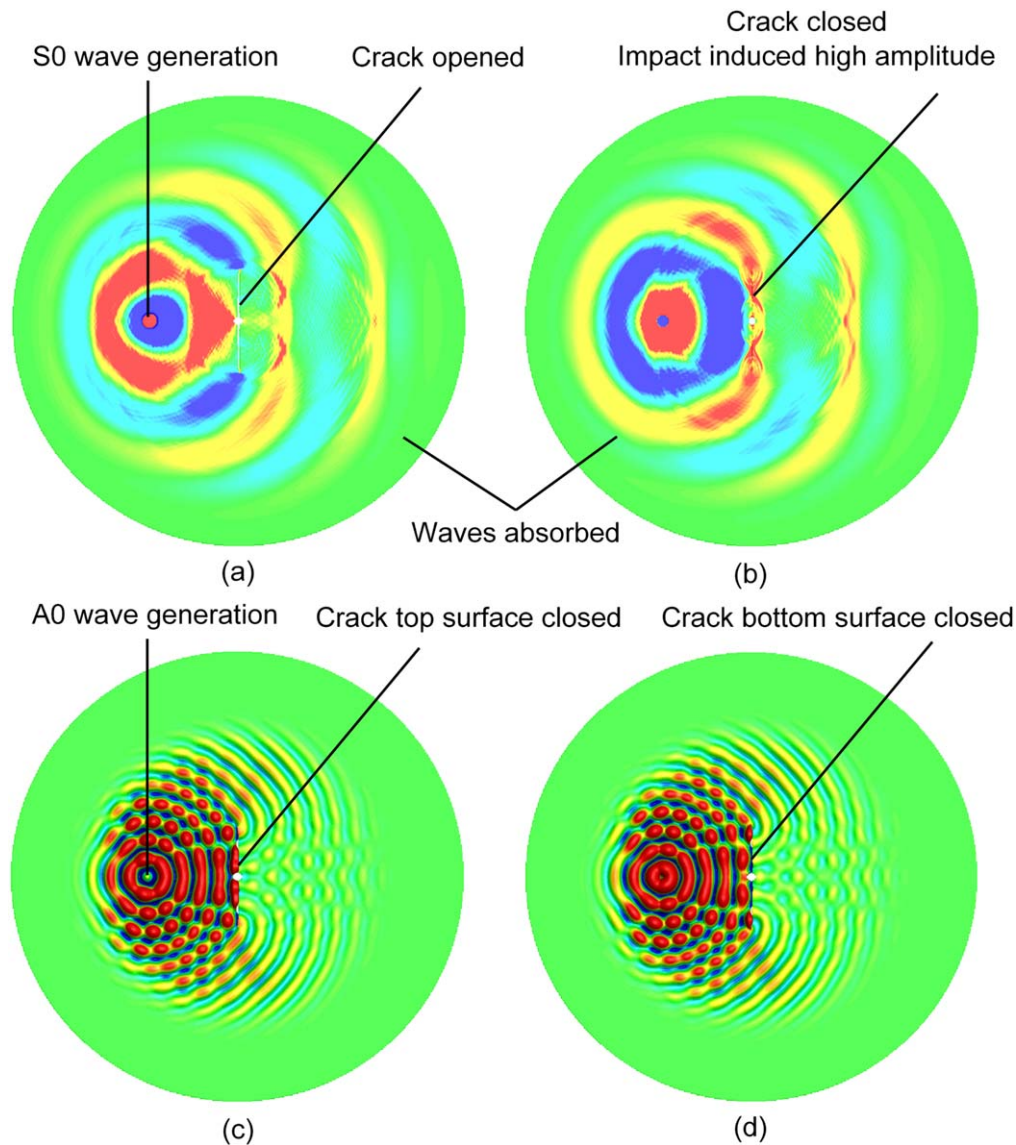
Figure 4. Predictive modeling results of nonlinear interactions between fundamental Lamb wave modes with the rivet hole and idealized breathing crack at 100 kHz: (a) S0 wave opens the crack; (b) S0 wave closes the crack with impact induced high amplitudes; (c) A0 wave closes the top surface of the crack; (d) A0 wave closes the bottom surface of the crack.

fundamental Lamb wave modes (S0 and A0) with the rivet hole and fatigue cracks under 100 kHz excitation using the small-size LISA model. Figure 4(a) shows the generation of S0 wave mode and its interaction with the fatigue crack by opening it up. While the compressional part of the S0 wave will close the crack surfaces as shown in figure 4(b). The impact between the crack interfaces induced high amplitude spikes in the wave field. The nonlinearity of the wave crack interactions arises from the periodic local stiffness change during the crack open and close contact dynamic procedure. Figures 4(c) and (d) present the generation of short-wavelength A0 Lamb mode into the structure and its interaction with the crack. Due to the antisymmetric motion of A0 mode across the plate thickness, the top and bottom crack surface will be opened and closed, taking turns in an alternative manner. It can also be noticed that the radiating guided wave fields are effectively absorbed by the ALID boundary.

Figure 5 presents the scattering coefficients for the case of S0 wave incidence at the rivet hole breathing crack. At the fundamental frequency of 100 kHz, the S0 incident waves were scattered as S0 mode and converted into SHS0 mode. However, no antisymmetric A0 Lamb mode was converted during the nonlinear scattering procedure. Similar mode conversion effect can be noticed for the second and the third harmonic scattering coefficients, i.e., when S0 wave interact with an idealized breathing crack, mode conversion only happened between the symmetric modes (S0 and SHS0), while the antisymmetric mode would not participate in the scattering and mode conversion procedure. Another important feature is the direction dependence of the scattering amplitude. At the fundamental frequency, the largest amplitude of scattered SHS0 mode happened around 25° and 150°, while the scattered S0 possessed the high amplitudes in 0° and 180° perpendicular to the crack line orientation. At the second and
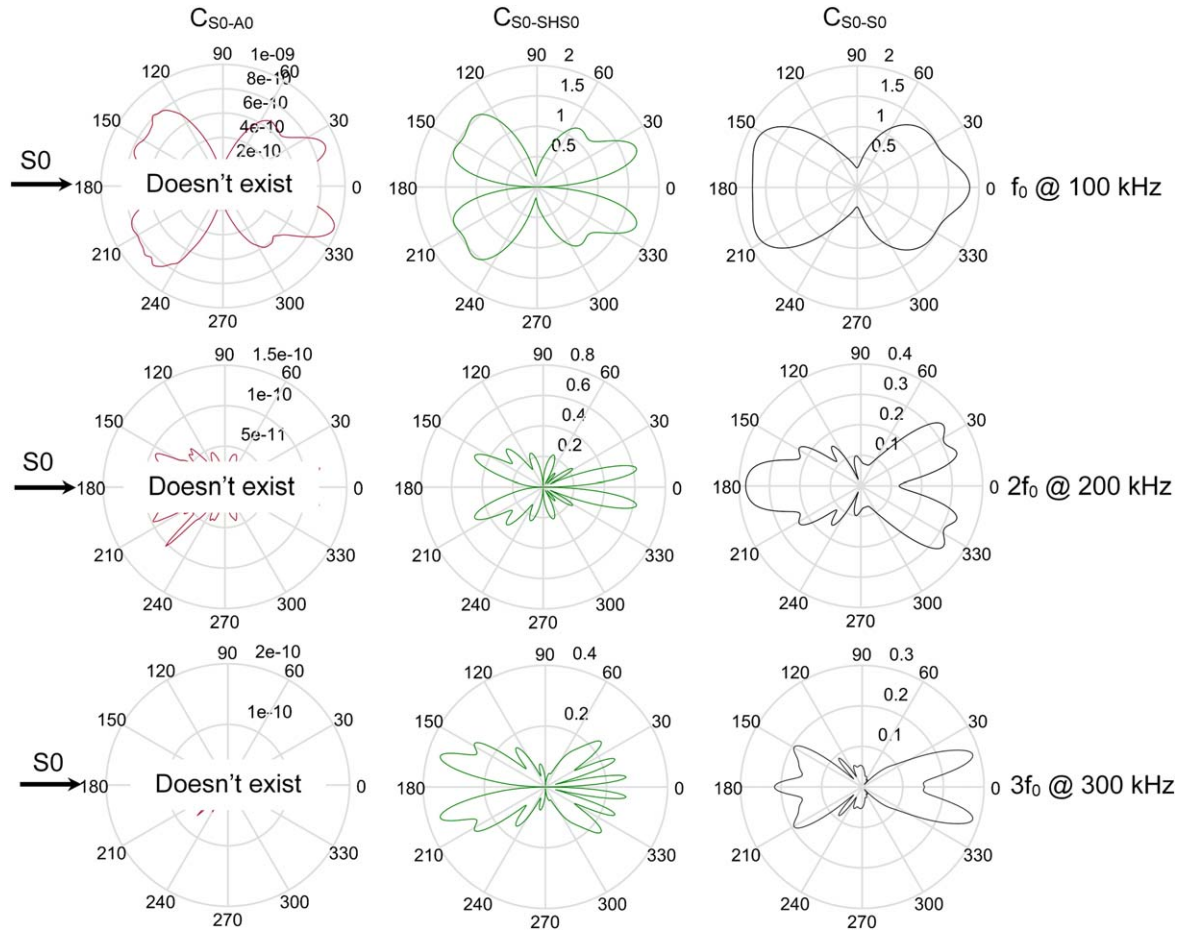
Figure 5. Scattering coefficients at the fundamental and superharmonic frequencies of incident S0 wave mode at 100 kHz for the breathing crack case.

third higher harmonic frequencies, however, the scattered S0 mode showed its highest forward amplitudes in 30° and 15° directions, respectively.

When A0 mode impinged on the breathing crack, the scattering pattern showed totally different behavior. Figure 6 shows that all the possible wave modes participated in the scattering procedure. At the fundamental frequency, the majority of the wave energy was scattered as A0 mode. Only a very small amount was converted to SHS0 and S0 modes. Nevertheless, the second harmonic frequency involved much less participation from A0, while SHS0 and S0 mode scattering amplitude gained much larger value. This indicates that the principal energy concentrated on the symmetric modes due to the mode conversion. Further, at the third harmonic frequency, A0 mode takes the majority of the scattering energy again, while the symmetric modes amplitude dropped significantly. Thus, the mode conversion phenomenon showed an alternating pattern between the antisymmetric and symmetric modes by taking up the principal scattering energy in turns. Such an alternating mode conversion feature is particularly special to the nonlinear scattering procedure. The linear interaction between guided waves and a through-thickness notch would not possess such distinctive mode conversion features.

The difference among the various wave modes at the fundamental and superharmonic frequency components comes from

the force and displacement matching condition at the crack interface. When the contact traction force distribution in the plate thickness direction agrees well with the corresponding wave mode shapes at the target frequencies, the corresponding wave modes will be favorably generated in a certain direction. Of course, to understand this, a complete mechanics and mathematical based analytical work is needed. To the authors' knowledge, such phenomena have been very well explained for linear wave damage interactions, such as the work conducted by Moreau *et al* as well as Poddar and Giurgiutiu [46, 47].

5. Nonlinear scattering considering rough crack surface condition

The analysis presented in the previous subsection is based on the assumption of an idealized breathing crack: the crack surfaces are smooth, in perfectly kissing contact condition with no pre-stresses nor initial gaps. However, a practical fatigue crack surface differs much from this idealized assumption. Such deviation may bring uncertainties and variation into the scattering procedure. Figure 7(a) shows the microscopic image of the fatigue crack. It can be observed that the crack surface is rough with a zigzag crack trace. At certain location, relatively large material voids can be seen, while at others the distance between the crack interfaces are
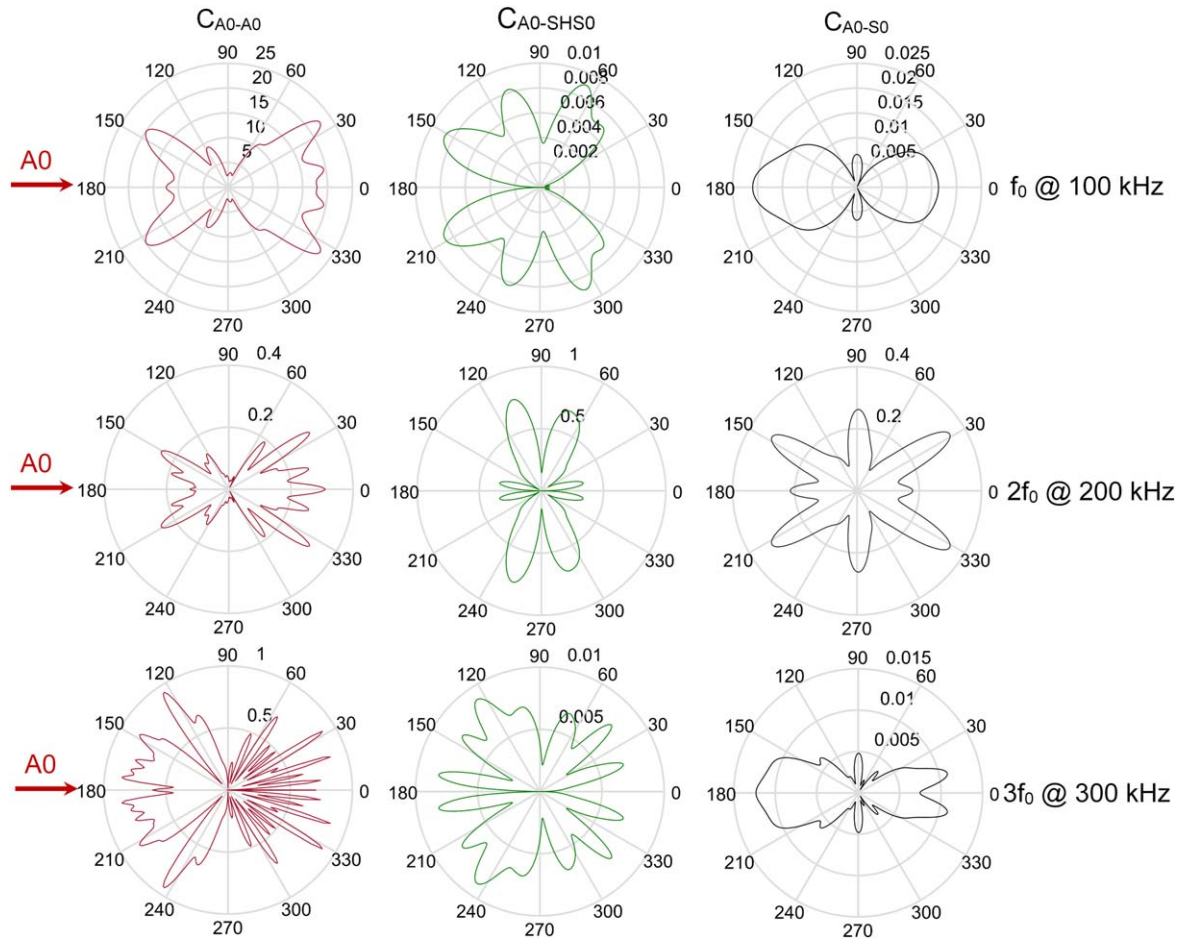
Figure 6. Scattering coefficients at the fundamental and superharmonic frequencies of incident A0 wave mode at 100 kHz for the breathing crack case.
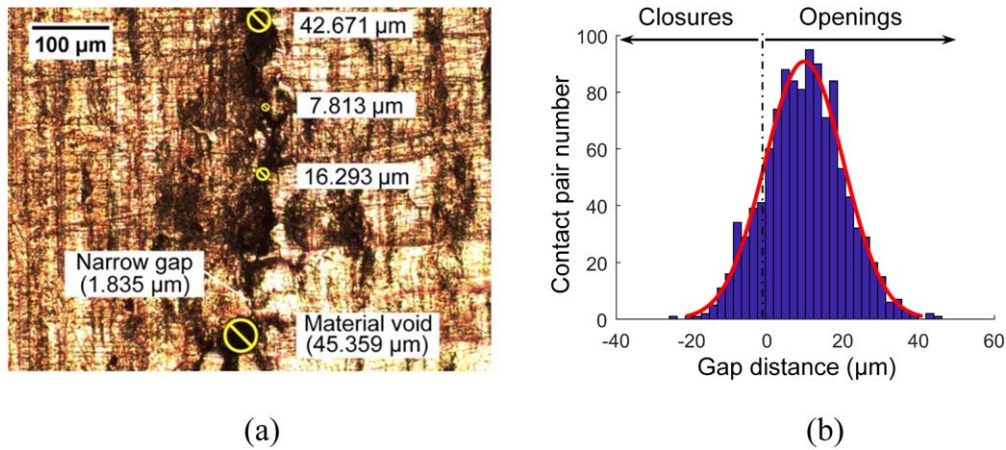

Figure 7. (a) Microscopic image of the fatigue crack; (b) assumed normal distribution of initial openings and closures at the rough crack interface.

much closer. Within the rough crack surface, initially closed areas also exist, indicating pre-stressed contact points. The initial openings and closures are distributed along the crack surface in a relatively random pattern. In order to capture the nature of such rough crack surfaces, randomly distributed initial gap functions were adopted for the contact pairs in the LISA model. Figure 7(b) presents the randomly generated

initial openings and closures along the crack contact surfaces following a normal distribution. A positive gap distance represents the initial openings and the negative gap distances corresponds to the initial closures with pre-stresses. The rough crack surface condition gives rise to the amplitude effect and random scattering directivity phenomenon. It will also influence the nonlinear resonance behavior during wave
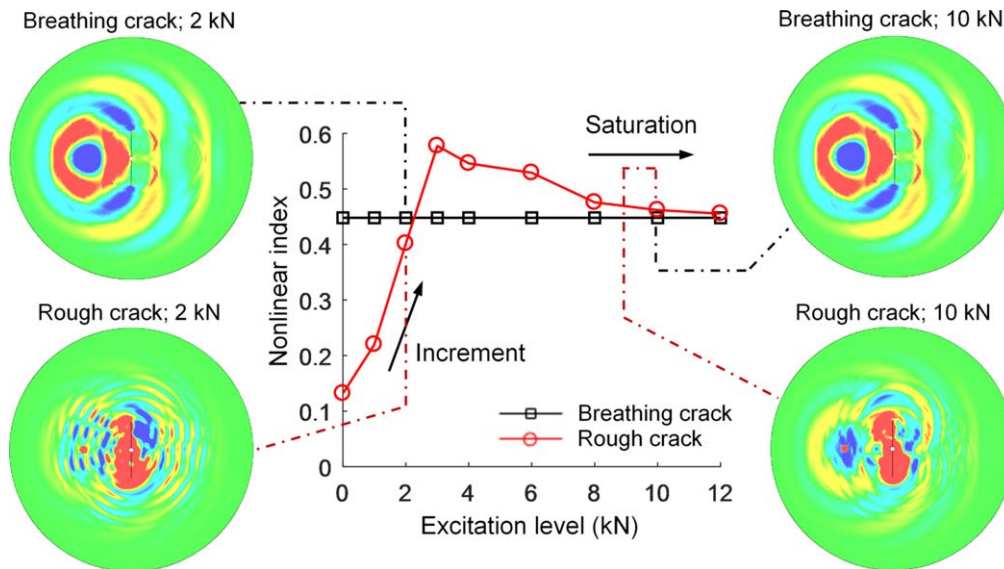
Figure 8. Signal nonlinearity and scattering pattern depends on the excitation amplitude for rough cracks; however, they stay the same for idealized breathing cracks.

crack interactions. It should be noted that it is very hard to capture the microscopic details of the 3D rough crack surfaces. Different gap/closure distributions will also result in totally distinctive scattering patterns. This study does not aim to obtain the scattering pattern for a specific crack. Instead, the emphasis focuses on the investigation of the general nonlinear scattering features and trends using a representative distribution function.

5.1. The mechanism of the amplitude effect in nonlinear guided wave scattering

Figure 8 presents the excitation amplitude influence on the ultrasonic guided wave scattering. The nonlinear index (NI) is plotted against the excitation level. The NI can be expressed as $NI = \sqrt{[A(2f_0) + A(3f_0)A(4f_0)]/A(f_0)}$, where $A(Nf_0)$ represents the Nth harmonic component amplitude. Quantitatively, it facilitates the measurement of the amplitude ratio between the superharmonic and the fundamental frequency components. Physically, it represents the nonlinear participation in the sensing signals.

For the idealized breathing crack case, the nonlinearity of the sensing signal does not depend on the excitation amplitude, i.e., the superharmonic and fundamental frequency components in the bi-linear oscillation response all undergo linearly proportional increment with the growth of the excitation amplitude. The nonlinear participation does not change. This is also evident from the identical wave propagation and scattering pattern shown in figure 8. On the other hand, for the rough crack case, when the excitation amplitude is low, the nonlinearity of the scattered waves is rather weak. With an increasing excitation amplitude, the nonlinearity of the wave field undergoes substantial increment. Beyond a certain level, the nonlinearity saturated and plateaued towards that of the idealized breathing crack case. This is because at low excitation level, only a small fraction of the contact pairs participated in the contact dynamic procedure due to the existence of initial gaps and closures. With larger

excitation amplitudes, more and more contact pairs will be engaged in the crack surface nonlinear interactions. One interesting phenomenon is that between 3 and 10 kN, the nonlinearity from the rough crack condition is stronger than that of the idealized breathing crack. This is because the contact points at the intermediate loading conditions allocate randomly along the crack surface. This may cause the superposition and interference of waves irradiating from these contact-point wave sources. Such a procedure may result in the enhancement of the nonlinear phenomenon at the sensing location. However, as the wave amplitude increases, the contact point distribution and force distribution even out. Thus, such interference effect disappears.

The numerically simulated wave fields in figure 8 also demonstrated that the scattering patterns differ much from each other for different excitation amplitudes. The example corresponds to the S0 wave incident situation. However, it is remarkable that the scattering patterns deviate much from the idealized breathing crack case. One obvious difference is that the scattered wave field now contains short wavelength A0 mode, indicating the mode conversion from S0 mode into A0 mode during the wave crack interactions. A second difference is that the scattered field becomes asymmetric or skewed. The third difference is that at various excitation levels, the scattering patterns appear to be totally dissimilar, i.e., the excitation amplitude changes the scattering feature.

To further illustrate the amplitude effect during the nonlinear scattering procedure as well as the difference between the idealized breathing crack model and the rough crack model, the in-plane displacements for the representative cases are also plotted in figure 9. It can be noticed that, for the breathing crack case, the only difference is the response amplitude, while the excitation amplitude does not exert any influence on the shape of the waveforms. On the other hand, for the rough crack case, the waveforms appear to be totally different. Such nonlinear amplitude influence may lay the foundation for a class of nonlinear ultrasonic SHM technique
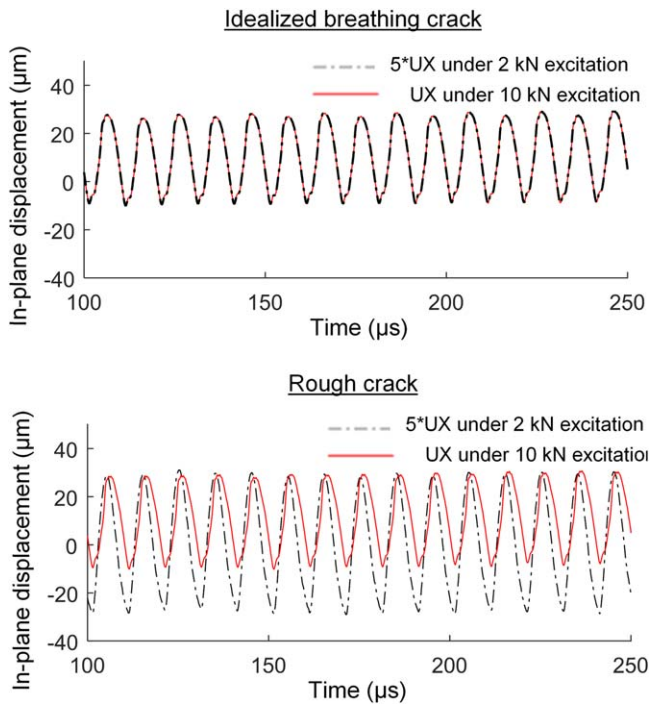
Idealized breathing crack

Rough crack

Figure 9. Nonlinear steady-state response for both the idealized breathing crack case and the rough crack case under two different load levels.
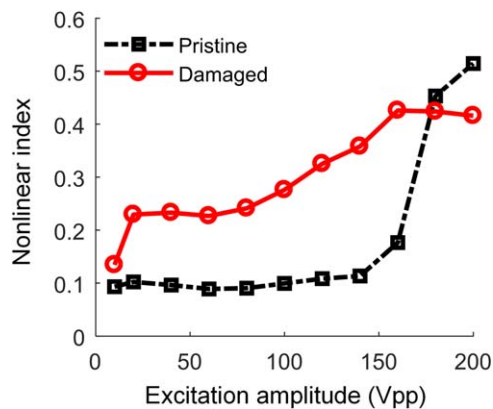

Figure 10. Experimental sensing signal nonlinear index versus excitation amplitude.

based on the amplitude dependent response. It can be concluded that the mechanism of the nonlinear amplitude effects for wave crack interactions stems from the rough crack surface condition. And the conventional bi-linear breathing crack model cannot capture such an important feature.

The amplitude dependent nonlinear trend was further compared with experimental measurements. The experiments were conducted for a pristine plate with a rivet hole and for a plate after the crack was nucleated from the rivet hole. Figure 10 shows that in the pristine plate, the nonlinearity of the sensing waves stayed at a considerably low level until the excitation amplitude increased up to 150 Vpp. At very high excitation amplitudes, the material nonlinearity manifested, such as the hysteresis behavior of the adhesive and the piezoelectric ceramic. The nonlinear indices of the damaged case, on the other

hand, underwent a monotonic increment up to 160 Vpp and plateaued. The trend of the experimental result agrees well with the predictive results as shown in figure 8, further illustrating the capability of our model in capturing the amplitude effect of nonlinear wave crack interactions. It should be noted that, after 180 Vpp, the nonlinearity in the pristine case surpassed that in the damaged case. This is due to the fact that higher harmonics with much higher frequencies and shorter wavelengths are more sensitive to the crack and are reflected back. On the other hand, the transmission of the super harmonic components in the pristine case are not influenced as much.

5.2. Random scattering pattern due to rough crack surface condition

To further demonstrate the influence of the crack roughness on the guided wave scattering pattern, the scattering coefficients are computed. Figure 11 presents the WDICs results of the scattered waves under a pair of 2 kN, out-of-phase, out-of-plane force excitation for S0 wave generation, which corresponds to the 'incremental' region for the NI. It can be observed that all possible wave modes participated in the scattering procedure. A0 mode was aroused from mode conversion, quite different from the selective mode conversion phenomena for idealized breathing crack case (figure 5), where the S0 mode can only be converted into symmetric modes (S0 and SHS0). Another remarkable difference is that the symmetry of the scattering pattern is broken. This is true for all the wave modes involved and especially obvious for the scattered A0 mode. The scattering coefficients take rather random patterns, which stems from the signature of the random initial opening and closure distribution along the crack line.

Figure 12 presents the scattering coefficient results under a pair of 10 kN excitation for S0 wave generation, which corresponds to the 'saturation' region for the NI. The scattering patterns differ much from the low amplitude excitation case (figure 11), indicating the amplitude effect during the nonlinear scattering procedure. One important phenomenon is that the scattering coefficients of SHS0 mode and S0 mode approach those in the idealized breathing crack case as shown in figure 5. However, the A0 mode still presents in the scattered wave field with considerable random patterns. Although the scattering amplitudes may take random patterns, the scattering coefficients along the crack line ($90°$ and $270°$) seem to be generally weak compared with other directions.

To validate such random scattering directivity effect, guided wave scattering experiments were performed on the specimens shown in figure 2. The $180°$ transducer performed as the transmitter generating guided waves into the structure. The other 23 transducers served as the sensors, picking up the ultrasonic response in every $15°$. Figure 13 presents the superharmonic scattering amplitude patterns under 10 and 100 Vpp excitations. It can be observed that the scattering patterns differ much from each other under the two excitation amplitudes, which validated the predictive phenomenon that the scattering patterns depends on wave amplitude. In addition, the experimental scattering patterns showed rather random directivity feature and the scattering amplitudes along the crack line direction are very weak,
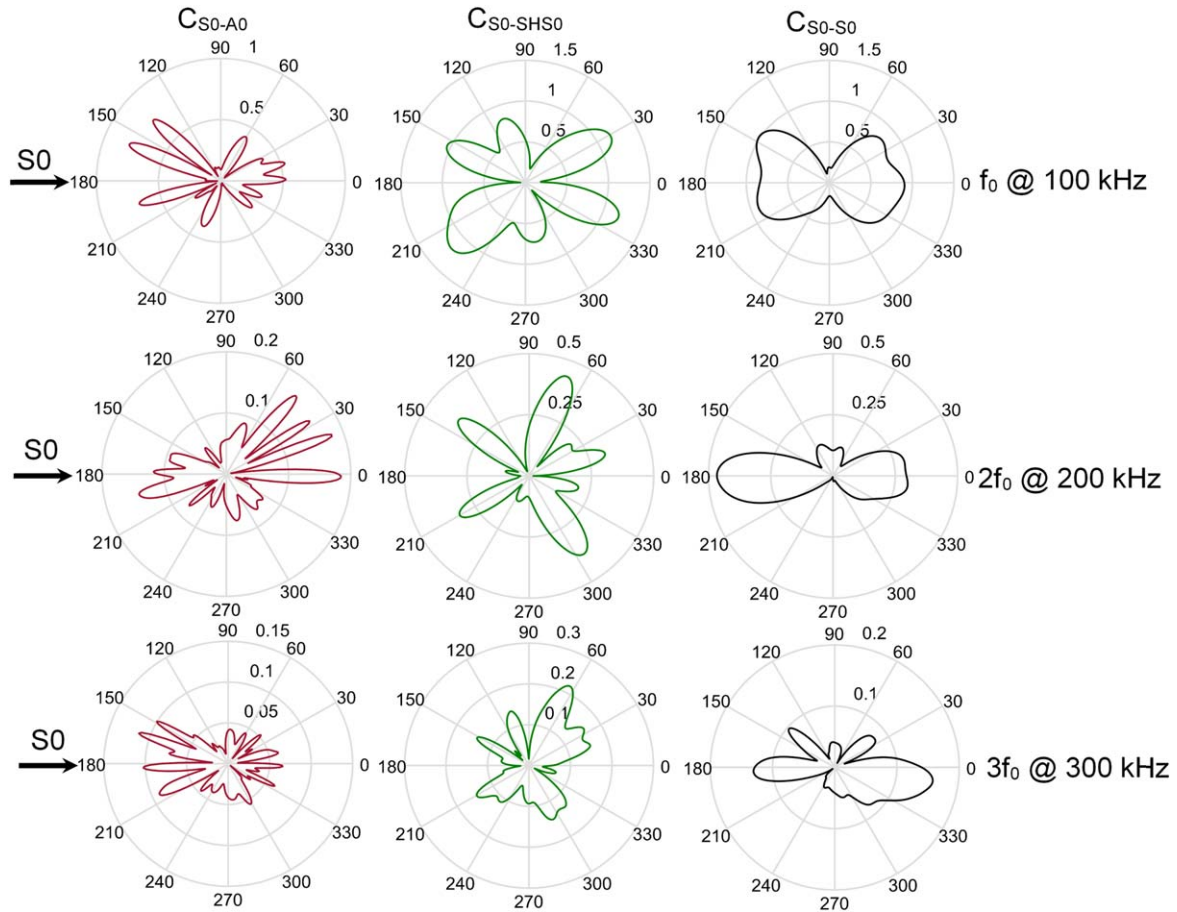
Figure 11. Scattering coefficients under a pair of 2 kN excitation for S0 wave generation.

which agrees with the predictive trends obtained using our numerical model.

It should be noted that it is easy to generate single mode Lamb waves and separate different modes in the scattered wave field in our LISA model. Different modes are examined in the numerical modeling case studies for the purpose of fundamental research of the nonlinear scattering phenomena. However, such selective wave mode generation and sensing remains a big challenge in the experiments. Some researchers adopted the transducer pairs bonded on top and bottom surfaces of the plates and exert in-phase or out-of-phase excitation on the piezo wafers to generate S0 or A0 waves. However, the quality of mode separation heavily depends on the unification of the individual transducer properties and sensor implementation quality. Even the single wave mode generation may be calibrated with very careful sensor selection, installation, and excitation amplitude tuning, it is hard to achieve for all the sensing pairs. A possible way of separating the wave modes in the sensing signals could be through the scanning laser vibrometry and frequency-wavenumber analysis. However, this will be considered in a future work and may be reported in an individual follow-up paper. In addition, the scattering patterns heavily depend on the details of the 3D rough surface condition and the distribution of the gap/closure. It is very difficult to capture all these microscopic details along such a long crack. In this study, a representative

distribution was adopted based on the data from the microscopic image of a small part of the crack. Thus, it is hard to compare the detailed scattering patterns between the LISA model and the experiments. Again, this study does not aim to obtain the scattering pattern for a specific crack. Instead, the emphasis focuses on the investigation of the general nonlinear scattering features and trends. It can be concluded that the general amplitude dependent behavior and the random scattering directivity pattern trends agree well between our predictive simulation results and the experiments.

5.3. The influence on nonlinear resonance behavior

In addition to the amplitude effects and random directivity of the nonlinear ultrasonic scattering, another important and special feature is the nonlinear resonance during wave crack interactions. At different excitation frequencies, the nonlinear response may vary much from each other. Within a certain frequency range, nonlinear superharmonic components may be much stronger, while within others the nonlinear higher harmonics can hardly be observed. The subharmonic resonances are even more sensitive to the excitation frequency. In order to investigate the influence of the rough crack condition on such nonlinear resonance effect, a chirp excitation sweeping from 50 kHz up to 250 kHz was used to generate S0 waves into the structure.
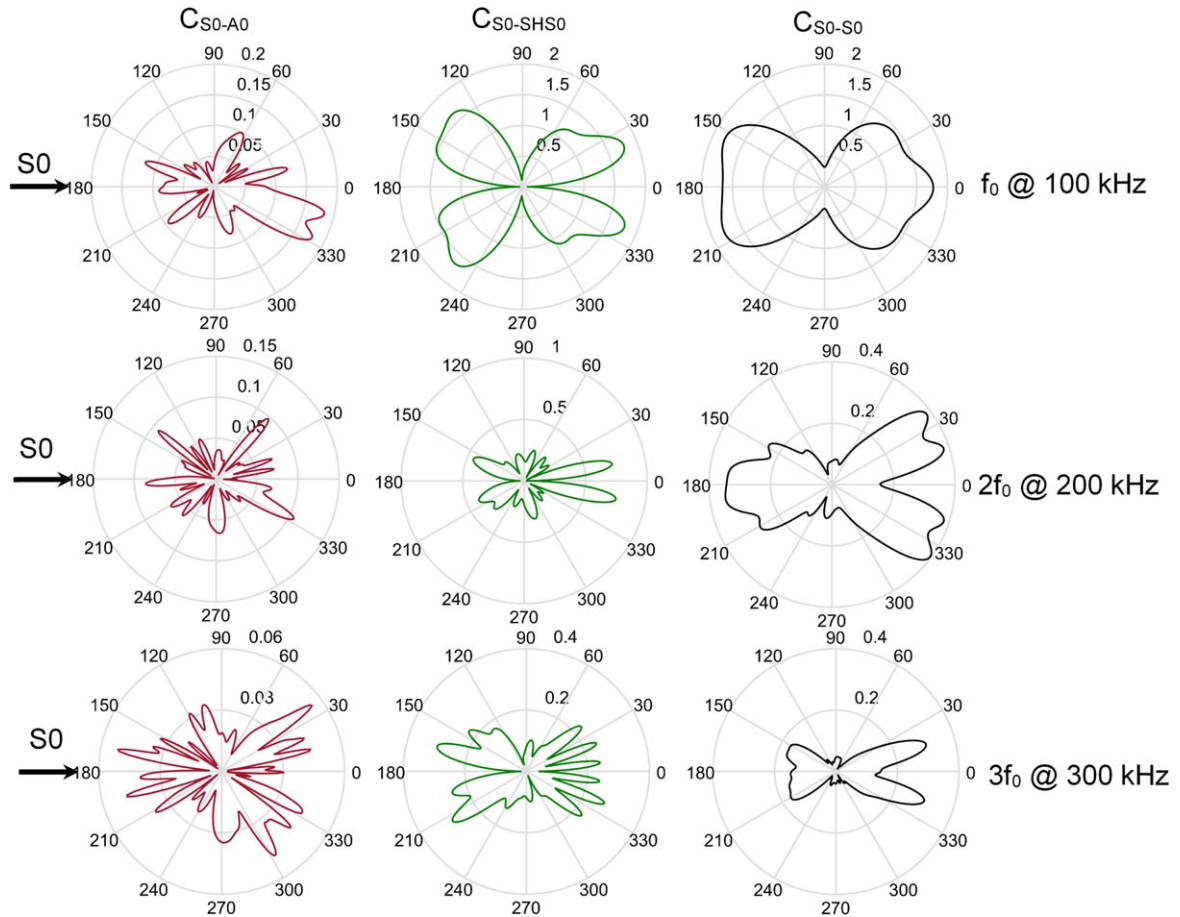
Figure 12. Scattering coefficients under a pair of 10 kN excitation for S0 wave generation.
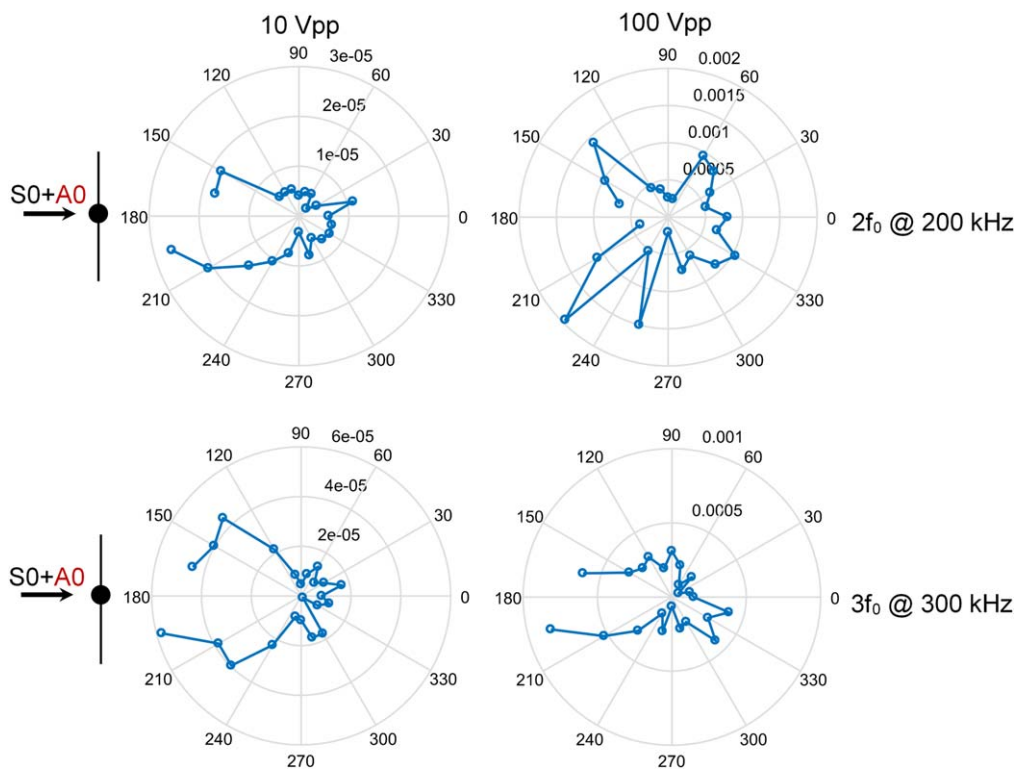

Figure 13. Experimental scattering patterns under different excitation amplitudes.
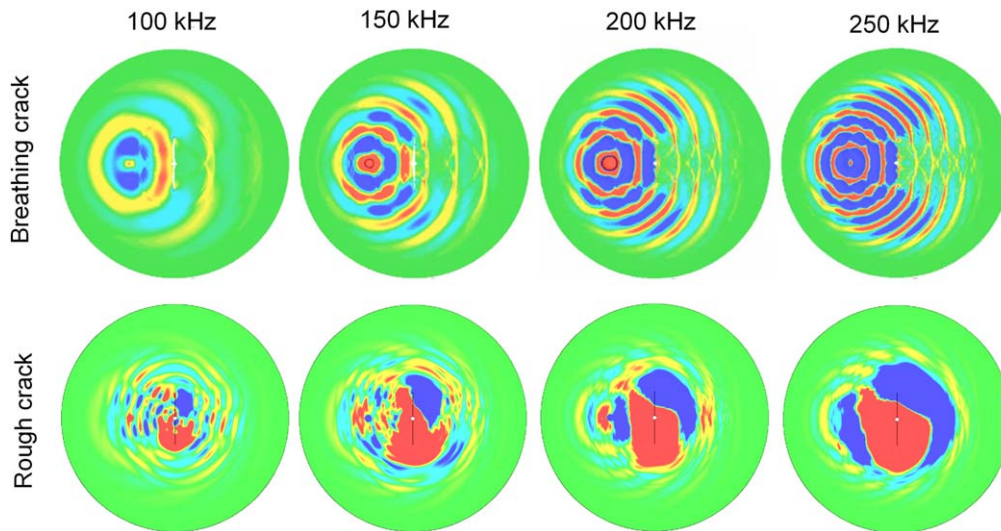
Figure 14. Wave damage interaction patterns under a frequency-sweeping excitation.
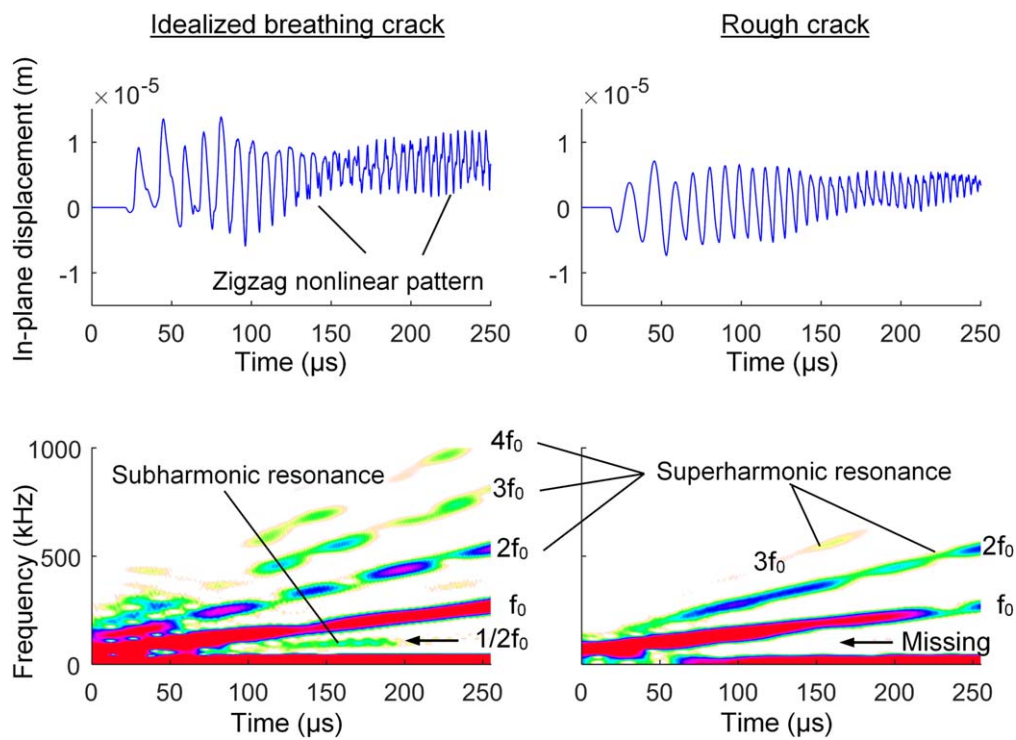

Figure 15. Frequency sweeping results of nonlinear subharmonic and superharmonic resonances using the numerical model; comparison between the idealized breathing crack case (left) and the rough crack case (right).

Figure 14 presents the wave damage interaction patterns under the frequency-sweeping excitation for both the idealized breathing crack case and the rough crack case. The out-of-plane displacement wave fields are plotted. For the breathing crack case, the superharmonic components with short wavelength can be clearly identified in the wave field. It can be observed that the amplitude and directivity appear to be much different at various frequencies. For the rough crack case, the random directivity scattering pattern and the mode converted, short-wavelength A0 mode can be clearly noticed. The low-frequency (DC) response is rather obvious in the out-of-plane displacement field. At different frequencies, the scattering pattern changed much as well.

Figure 15 presents the predictive in-plane displacement 50 mm behind the crack. The time traces of the sensing signals and their time–frequency analysis are shown for both the idealized breathing crack case and the rough crack case. The zigzag nonlinear response pattern can be clearly noticed in the sensing signals. It shows that in addition to the fundamental frequency ramping up with time, DC component and superharmonic resonances also showed up. It should be noted that the amplitude of the superharmonics are not constant throughout the frequency range, possessing humps and valleys, indicating the resonance phenomenon. A special subharmonic resonance can also be observed around 160 μs, corresponding to
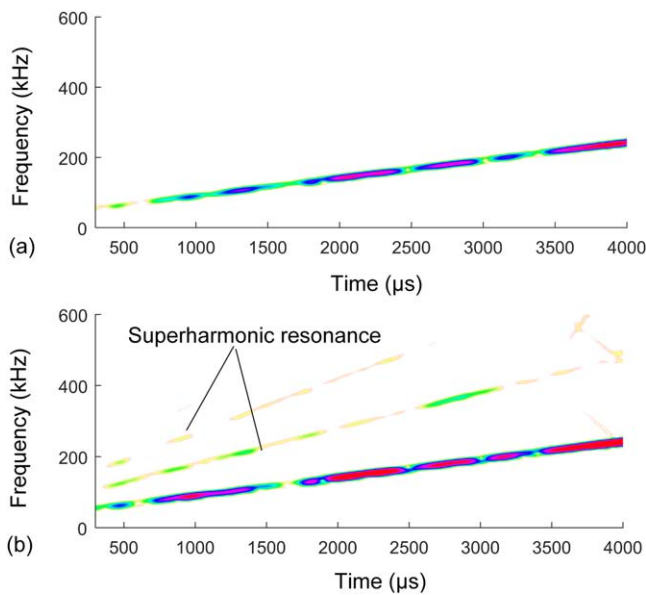
Figure 16. Experimental results of frequency sweeping tests: (a) time–frequency spectrum under 10 Vpp excitation; (b) time–frequency spectrum under 100 Vpp excitation.

approximately 180–190 kHz excitation for the idealized breathing crack case. The subharmonic resonance is very sensitive to the excitation frequency and the local resonant frequency of the damage itself. For the rough crack case, the subharmonic resonance is missing. The superharmonic resonances are also much weaker compared with those in the breathing crack case. For example, the 4th order superharmonic is very weak and barely visible. This highlighted the influence of the rough crack condition on the nonlinear resonance phenomenon.

The frequency sweeping experiments on the fatigue specimen were also performed. Figure 16(a) shows the experimental result when a 10 Vpp excitation amplitude was used. It can be seen that only the fundamental excitation frequency component was present. Figure 16(b) shows the frequency sweeping result under a 100 Vpp excitation. Distinctive superharmonics can be clearly noticed. The superharmonic components also showed similar resonant behaviors as predicted by our numerical analysis for the rough crack. The 4th order superharmonic component is very weak. The subharmonic resonance is missing as predicted in the numerical results. In addition, the resonant frequencies also do not match exactly between experiments and our model. This is due to the fact that the microscopic rough feature of the crack interfaces will influence the dynamic behavior of the crack. The excitation amplitude would further affect the nonlinear response. It is hard to capture the extensive details of the fatigue crack. Nevertheless, the numerical analysis is still indicative and can provide insights into the understanding of the physical phenomena.

To demonstrate the existence of subharmonic resonance, with its considerable sensitivity to the excitation profile, experiments on the fatigue specimen were performed by carefully tuning a 100 Vpp continuous harmonic excitation

between 180 and 190 kHz. Around 185.2 kHz, the subharmonic resonance was observed. Figure 17(a) shows the frequency spectrum of the excitation, containing only the excitation frequency at 185.2 kHz. Figure 17(b) presents the frequency-domain response after the wave crack interaction. In addition to the fundamental frequency at $f_0 = 185.2$ kHz, the subharmonic component around 93.27 kHz was also clearly noticed. Sideband frequency component at $f_0 + 1/2 f_0$ showed up as well due to the mixed frequency response or the so-called wave modulation. Superharmonics also appeared at $2f_0$, $3f_0$, etc. It should be pointed out that in both figures 15(b) and 16(b), the subharmonic component was not observed for the rough crack case. This is because the sweeping chirp excitation was used. The results shown in figure 17 was obtained using a continuous harmonic excitation. The existence condition for the subharmonic resonance is quite demanding. The excitation frequency and amplitude matching condition must be strictly satisfied. Such existence condition has been discussed by Zhang *et al*, where they showed the existence condition followed a 'V' shape profile defined by the excitation frequency and amplitude [48].

6. Concluding remarks and future work

This article presented the investigation of nonlinear scattering features of guided waves from rivet hole nucleated fatigue cracks. A small-size LISA model was tailored for the efficient analysis of the scattering procedure. Active sensing experiments were performed to study the nonlinear features during wave crack interactions. The influence of the rough crack surface condition on several distinctive aspects of the nonlinear scattering phenomenon were discussed: (1) the amplitude effect; (2) the directivity and mode conversion features; (3) the nonlinear resonance phenomenon.

Our investigation started with the idealized breathing crack model. Quantitative analysis was conducted and the scattering coefficients were obtained. It was found that the incident S0 mode would only be scattered as symmetric modes (S0 and SHS0). No A0 waves were present in the scattered wave field. When A0 mode impinged on the breathing crack, all the possible wave modes would participate in the scattering procedure. However, it showed a special selective alternating participation phenomenon between the antisymmetric and symmetric modes.

Next, the rough crack surface model was used to show the amplitude effect and random feature during the ultrasonic nonlinear scattering procedure. The emphasis was put on illustrating the difference between the breathing crack and rough crack responses. The analysis showed that the nonlinearity of the guided waves grew with the increasing excitation amplitude for the rough crack. However, no amplitude dependence was noticed for the breathing crack case. The amplitude dependent nonlinear trend was compared with experimental measurements. The numerical predictive trend agrees well with the experimental data.
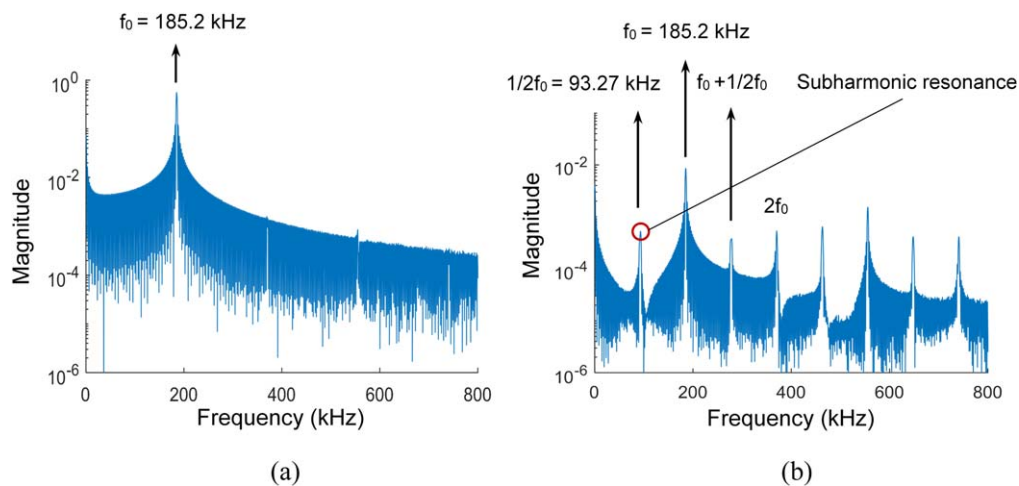
Figure 17. Subharmonic resonance spectrum under 185.2 kHz excitation: (a) excitation containing only the fundamental frequency; (b) nonlinear response with subharmonic, sideband, and superharmonic resonances. (Note the subharmonic resonance happened at 93.27 kHz.)

The scattering patterns also showed skewed shapes which also differed from each other under various excitation amplitudes. The random scattering directivity and mode conversion effects were observed for the rough crack case. All the possible wave modes would participate in the scattering procedure. However, the breathing crack case showed symmetric scattering patterns and selective mode conversion phenomena. The phenomenological features and trends from the predictive simulations were validated using the active sensing experiments on the fatigue specimen.

Finally, the influence from the rough crack condition on the nonlinear resonance phenomenon was investigated by conducting the frequency sweeping tests using both the numerical model and the experiments. It was found that superharmonic and subharmonic resonances exist at various frequency ranges for the breathing crack case. However, for the rough crack case, the superharmonic resonances are weaker and the subharmonic resonance was missing. The experiment showed that the resonances were also amplitude dependent. In addition, the existence condition for the subharmonic resonance was quite demanding. The excitation frequency and amplitude matching condition must be satisfied. All these special features of nonlinear ultrasonic scattering may provide insights and guidelines for nonlinear guided wave based SHM system design.

For future work, nonlinear guided wave SHM methods should be explored based on the special features of the nonlinear scattering procedure, such as amplitude based technique, nonlinear resonance spectrum technique, and the visual based nonlinear laser imaging methods. The laser vibrometry and wavenumber analysis should be explored to experimentally evaluate the mode conversion phenomenon during nonlinear wave scattering.

ORCID iDs

Yanfeng Shen ⓘ https://orcid.org/0000-0002-3025-4664

References

[1] Su Z, Zhou C, Hong M, Cheng L, Wang Q and Qing X 2014 Acousto-ultrasonics-based fatigue damage characterization: linear versus nonlinear signal features *Mech. Syst. Signal Process.* **45** 225–39

[2] Dutta D, Sohn H, Harries K A and Rizzo P 2009 A nonlinear acoustic technique for crack detection in metallic structures *Struct. Health Monit., Int. J.* **8** 251–62

[3] Alleyne D and Cawley P 1992 The interaction of Lamb waves with defects *IEEE Trans. Ultrason. Ferroelectr. Freq. Control* **39** 381–97

[4] Rose J, Ditri J, Pilarski A, Rajana K and Carr F 1994 A guided wave inspection technique for nuclear steam generator tubing *NDT&E Int.* **27** 307–10

[5] Kundu T, Maslov K, Karpur P, Matikas T and Nicolaou P 1996 A Lamb wave scanning approach for the mapping of defects in [0/90] titanium matrix composites *Ultrasonics* **34** 43–9

[6] Maslov K and Kundu T 1997 Selection of Lamb modes for detecting internal defects in composite laminates *Ultrasonics* **35** 141–50

[7] Ghosh T, Kundu T and Karpur P 1998 Efficient use of Lamb modes for detecting defects in large plates *Ultrasonics* **36** 791–801

[8] Yang W and Kundu T 1998 Guided waves in multilayered anisotropic plates for internal defect detection *ASCE J. Eng. Mech.* **124** 311–8

[9] Jung Y, Kundu T and Ehsani M 2001 Internal discontinuity detection in concrete by Lamb waves *Mater. Eval.* **59** 418–23

[10] Na W and Kundu T 2002 Underwater pipeline inspection using guided waves *Trans. ASME, J. Press. Vessel Technol.* **124** 196–200

[11] Vasiljevic M, Kundu T, Grill W and Twerdowski E 2008 Pipe wall damage detection by electromagnetic acoustic transducer generated guided waves in absence of defect signals *J. Acoust. Soc. Am.* **123** 2591–7

[12] Ahmad R, Banerjee S and Kundu T 2009 Pipe wall damage detection in buried pipes using guided waves *ASME J. Press. Vessel Technol.* **131** 011501

[13] Fromme P 2013 Noncontact measurement of guided ultrasonic wave scattering for fatigue crack characterization *SPIE Smart Structures and NDE (San Diego)*

[14] Chan H, Masserey B and Fromme P 2015 High frequency guided ultrasonic waves for hidden fatigue crack growth monitoring in multi-layer model aerospace structures *Smart Mater. Struct.* **24** 1–10

[15] Chen X, Michaels J E and Michaels T E 2015 A methodology for estimating guided wave scattering patterns from sparse transducer array measurements *IEEE Trans. Ultrason. Ferroelectr. Freq. Control* **62** 208–19

[16] Masserey B and Fromme P 2017 Analysis of high frequency guided wave scattering at a fastener hole with a view to fatigue crack detection *Ultrasonics* **76** 78–86

[17] Quaegebeur N, Bouslama N, Bilodeau M, Guitel R, Masson P, Maslouhi A and Micheau P 2017 Guided wave scattering by geometrical change or damage: application to characterization of fatigue crack and machined notch *Ultrasonics* **73** 187–95

[18] Klepka A, Staszewski W, Jenal R, Szwedo M, Iwaniec J and Uhl T 2011 Nonlinear acoustics for fatigue crack detection —experimental investigations of vibro-acoustic wave modulations *Struct. Health Monit., Int. J.* **11** 197–211

[19] Chen X, Michaels J, Lee S and Michaels T 2012 Load-differential imaging for detection and localization off atigue cracks using Lamb waves *NDT&E Int.* **51** 142–9

[20] Hong M, Su Z, Lu Y, Sohn H and Qing X 2015 Locating fatigue damage using temporal signal features of nonlinear Lamb waves *Mech. Syst. Signal Process.* **60** 182–97

[21] Wu W, Qu W, Xiao L and Inman D 2016 Detection and localization of fatigue crack with nonlinear instantaneous baseline *J. Intell. Mater. Syst. Struct.* **27** 1577–83

[22] Liu P, Sohn H, Kundu T and Yang S 2014 Noncontact detection of fatigue cracks by laser nonlinear wave modulation spectroscopy (LNWMS) *NDT&E Int.* **66** 106–16

[23] Liu P, Sohn H and Park B 2015 Baseline-free damage visualization using noncontact laser nonlinear ultrasonics and state space geometrical changes *Smart Mater. Struct.* **24** 1–13

[24] Lim H, Kim Y, Koo G, Yang S, Sohn H, Bae I and Jang J 2016 Development and field application of nonlinear ultrasonic modulation technique for fatigue crack detection without reference data from an intact condition *Smart Mater. Struct.* **25** 1–14

[25] Cheng J, Potter J, Croxfold A and Drinkwater B 2017 Monitoring fatigue crack growth using nonlinear ultrasonic phased array imaging *Smart Mater. Struct.* **26** 1–10

[26] Broda D, Staszewski W, Martowicz A, Uhl T and Silberschmidt V 2014 Modelling of nonlinear crack–wave interactions for damage detection based on ultrasound—a review *J. Sound Vib.* **333** 1097–118

[27] Shen Y and Giurgiutiu V 2014 Waveformrevealer: an analytical framework and predictive tool for the simulation of multi-modal guided wave propagation and interaction with damage *Struct. Health Monit., Int. J.* **13** 491–511

[28] Shen Y and Giurgiutiu V 2013 Predictive modeling of nonlinear wave propagation for structural health monitoring with piezoelectric wafer active sensors *J. Intell. Mater. Syst. Struct.* **25** 506–20

[29] Hirose S 1994 2D Scattering by a crack with contact-boundary coditions *Wave Motion* **19** 37–49

[30] Poznic M and Pecorari C 2005 Nonlinear scattering by a partially closed surface breaking crack *Review of Quantitatie Nondestructive Evaluation*

[31] Blanloeuil P, Meziane A, Norris A and Bacon C 2016 Analytical extension of finite element solution for computing the nonlinear far field of ultrasonic waves scattered by a closed crack *Wave Motion* **66** 132–46

[32] Blanloeuil P, Rose L R F, Guinto J, Veidt M and Wang C 2016 Closed crack imaging using time reversal method based on fundamental and second harmonic scattering *Wave Motion* **66** 156–76

[33] Wang K and Su Z 2016 Analytical modeling of contact acoustic nonlinearity of guided waves and its application to evaluating severity of fatigue damage *SPIE Conf. Proc. (Las Vegas)*

[34] Wang K and Su Z 2017 A three-dimensional analytical model for interpreting contact acoustic nonlinearity generated by a breathing crack in plate *SPIE Conf. Proc.* (Portland)

[35] Hafezi M H, Alebrahim R and Kundu T 2017 Peri-ultrasound for modeling linear and nonlinear ultrasonic response *Ultrasonics* **80** 47–57

[36] Hafezi M and Kundu T 2018 Peri-ultrasonic modeling of dynamic response of an interface crack showing wave scattering and crack propgation *J. Nondestruct. Eval., Diagn. Prognostics Eng. Syst.* **1** 1–6

[37] He S and Ng C 2017 Modelling and analysis of nonlinear guided waves interaction at a breathing crack using time-domain spectral finite element method *Smart Mater. Struct.* **26** 1–15

[38] Shen Y and Cesnik C 2017 Modeling of nonlinear interactions between guided waves and fatigue cracks using local interaction simulation approach *Ultrasonics* **74** 106–23

[39] Shen Y and Cesnik C 2018 Local interaction simulation approach for efficient modeling of linear and nonlinear ultrasonic guided wave active sensing of complex structures *J. Nondestruct. Eval., Diagn. Prognostics Eng. Syst.* **1** 1–9

[40] Radecki R, Su Z, Cheng L, Packo P and Staszewski W 2018 Modelling nonlinearity of guided ultrasonic waves in fatigued materials using a nonlinear local interaction simulation approach and a spring model *Ultrasonics* **84** 272–89

[41] Zhang J, Drinkwater B and Wilcox P 2011 Longitudinal wave scattering from rough crack-like defects *IEEE Trans. Ultrason. Ferroelectr. Freq. Control* **58** 2171–80

[42] Nadella K and Cesnik C 2013 Local interaction simulation approach for modeling wave propagation in composite structures *CEAS Aeronaut. J.* **4** 35–48

[43] Shen Y and Giurgiutiu V 2015 Effective non-reflective boundary for Lamb waves: theory, finite element implementation, and applications *Wave Motion* **58** 22–41

[44] Shen Y and Giurgiutiu V 2016 Combined analytical FEM approach for efficient simulation of Lamb wave damage detection *Ultrasonics* **69** 116–28

[45] Shen Y and Cesnik C 2016 Efficient modeling of nonlinear scattering of ultrasonic guided waves from fatigue cracks using local interaction simulation approach *ASME 2016 Int. Mechanical Engineering Congress and Exposition (Phoenix)*

[46] Moreau L, Caleap M, Velichko A and Wilcox P D 2012 Scattering of guided waves by flat-bottomed cavities with irregular shapes *Wave Motion* **49** 375–87

[47] Poddar B and Giurgiutiu V 2016 Complex modes expansion with vector projection using power flow to simulate Lamb waves scattering from horizontal cracks and disbonds *J. Acoust. Soc. Am.* **140** 2123–33

[48] Zhang M, Shen Y, Xiao L and Qu W 2017 Application of subharmonic resonance for the detection of bolted joint looseness *Nonlinear Dyn.* **88** 1–11